Catalytic Domain Structure of Vampire Bat Plasminogen Activator: A Molecular Paradigm for Proteolysis without Activation Cleavage

Martin Renatus,*,‡ Milton T. Stubbs,‡,§ Robert Huber,‡ Peter Bringmann,|| Peter Donner,|| Wolf-Dieter Schleuning,|| and Wolfram Bode*,‡

Department of Structural Research, Max-Planck-Institute of Biochemistry, D-82152 Martinsried, Germany, and Research Laboratories, Schering AG, Müllerstrasse 170-178, D-13342 Berlin, Germany

Received May 14, 1997⊗

ABSTRACT: The saliva of the blood-eating vampire bat *Desmodus rotundus* contains plasminogen activators (PAs) that maintain the fluidity of the prey's blood by activating plasminogen and dissolving developing fibrin clots. *D. rotundus* salivary PAs (DSPAs) are composed of evolutionarily conserved domains reminiscent of human tissue-type PA (tPA), but their catalytic domain lacks a plasmin-sensitive "activation cleavage site". Despite this, all DSPAs are intrinsically active and enormously stimulated in the presence of fibrin. The recombinant catalytic domain of DSPAα_1 has been crystallized in a covalent complex with Glu-Gly-Arg-chloromethyl ketone and its structure solved at 2.9 Å resolution. The structure is similar to that of activated two-chain human tPA. Despite its single-chain status, the activation domain is observed in an enzymatically active conformation, with a functional substrate binding site and active site accommodating the peptidylmethylene inhibitor. The activation pocket, which normally receives the N-terminal Ile16, is occupied by the side chain of Lys156, whose distal ammonium group makes an internal salt bridge with the carboxylate group of Asp194. Lys156 is in a groove shielded from the bulk solvent by the intact "activation loop" (Gln10−Phe21), favoring Lys156−Asp194 salt bridge formation and stabilization of a functional substrate binding site. Together with the characteristic 186 insertion loop, the activation loop could act as a switch, effecting full single-chain enzymatic activity upon binding to fibrin.

The vampire bat *Desmodus rotundus* is unique among vertebrates in being exclusively dependent on a diet of fresh blood. The saliva of vampire bats contains a variety of proteins which act to satisfy two essential requirements: the maintenance of prolonged bleeding from the wound and the preservation of blood fluidity after its ingestion. In contrast to those of lower hematophageous animals, which prevent coagulation for the purpose of sucking blood (*3*), plasminogen activators appear to be the predominant modulators of haemostasis in vampire bat saliva (*4*). By activating plasminogen to plasmin, DSPAs[1] (*D. rotundus* plasminogen activators) induce fibrinolysis, allowing simultaneous formation and degradation of small fibrin clots. Inhibitors of platelet aggregation and blood coagulation have also been reported (*5*). The slow bleeding afforded by weak inhibition of the clotting system enables the vampire bat to feed by licking blood from an open wound of the prey.

Four distinct plasminogen activators have been identified in the vampire bat salivary gland (*6*, *7*). DSPAα_1 and -α_2 are large (477 amino acids) molecules containing four distinct modules: a finger domain F, an epidermal growth factor like domain E, a kringle domain K, and a serine proteinase domain P. The smaller truncated forms DSPAβ and -γ lack the finger domain or finger-EGF tandem, respectively (*6*, *7*). All isoenzymes contain a catalytic domain harboring the active site residues His57-Asp102-Ser195[2] and are homologous to other chymotrypsin-like serine proteinases, in particular to human tissue-type plasminogen activator (tPA) (*6*, *7*) (see Table 1).

Surprisingly, the catalytic domain of DSPA lacks a plasmin-sensitive activation cleavage site. This is in contrast to all other functional members of the chymotrypsin family (mammalian origin), including human tPA, which are secreted as zymogen forms but are converted into a more active form by activation cleavage. Despite an intact active site, these precursors are for the most part inactive due to partial obstruction/disorder of the specificity pocket and malformation of the oxyanion hole (*8*−*12*). In the normal course of activation, the peptide bond between Arg15 (or Lys15) and Ile16 (or Val16) [chymotrypsinogen numbering (*13*)] is cleaved to give rise to a new N-terminal segment NH_3^+-Ile/Val16-Xxx-Xxx-Gly19. This segment inserts into the body of the proteinase, allowing formation of a buried salt bridge between the free amino terminus and the carboxylate group of Asp194, which is relocated from a

* Corresponding authors. Telephone: +49-(0)89-8578-2678. Fax: +49-(0)89-8578-3516. E-mail: renatus@biochem.mpg.de and bode@biochem.mpg.de.

‡ Max-Planck-Institute of Biochemistry.

§ Present address: Institute for Pharmaceutical Chemistry, Philipps-University Marburg, Marbacher Weg 6, D-35032 Marburg, Germany.

|| Schering AG.

⊗ Abstract published in *Advance ACS Abstracts,* October 1, 1997.

[1] Abbreviations: PAs, plasminogen activators; DSPAs, *D. rotundus* plasminogen activators; tPA, tissue-type plasminogen activator; uPA, urokinase-type plasminogen activator; PAI, plasminogen activator inhibitor; sc, one-chain; tc, two chain; P, protease domain or catalytic domain; tc-tPA(bisb), catalytic domain of activated tissue-type plasminogen activator in complex with the bisbenzamidine inhibitor 2,7-bis(4-amidinobenzylidene)cycloheptan-1-one (*1*); tc-tPA(ba), catalytic domain of activated tissue-type plasminogen activator in complex with benzamidine inhibitor (*2*).

[2] Residues are numbered using the chymotrypsinogen numbering, based on the topological equivalence of the proteolytic domain of DSPA with chymotrypsinogen (see ref 2).

S0006-2960(97)01129-X CCC: $14.00

Table 1: Sequence Alignment of the Catalytic Domains of DSPAα_1, DSPAα_2, Human tPA, and Human uPA and the Enzymes Bovine Trypsin and Bovine Chymotrypsinogen A Based on the Topological Equivalence with Bovine Chymotrypsinogen[a]

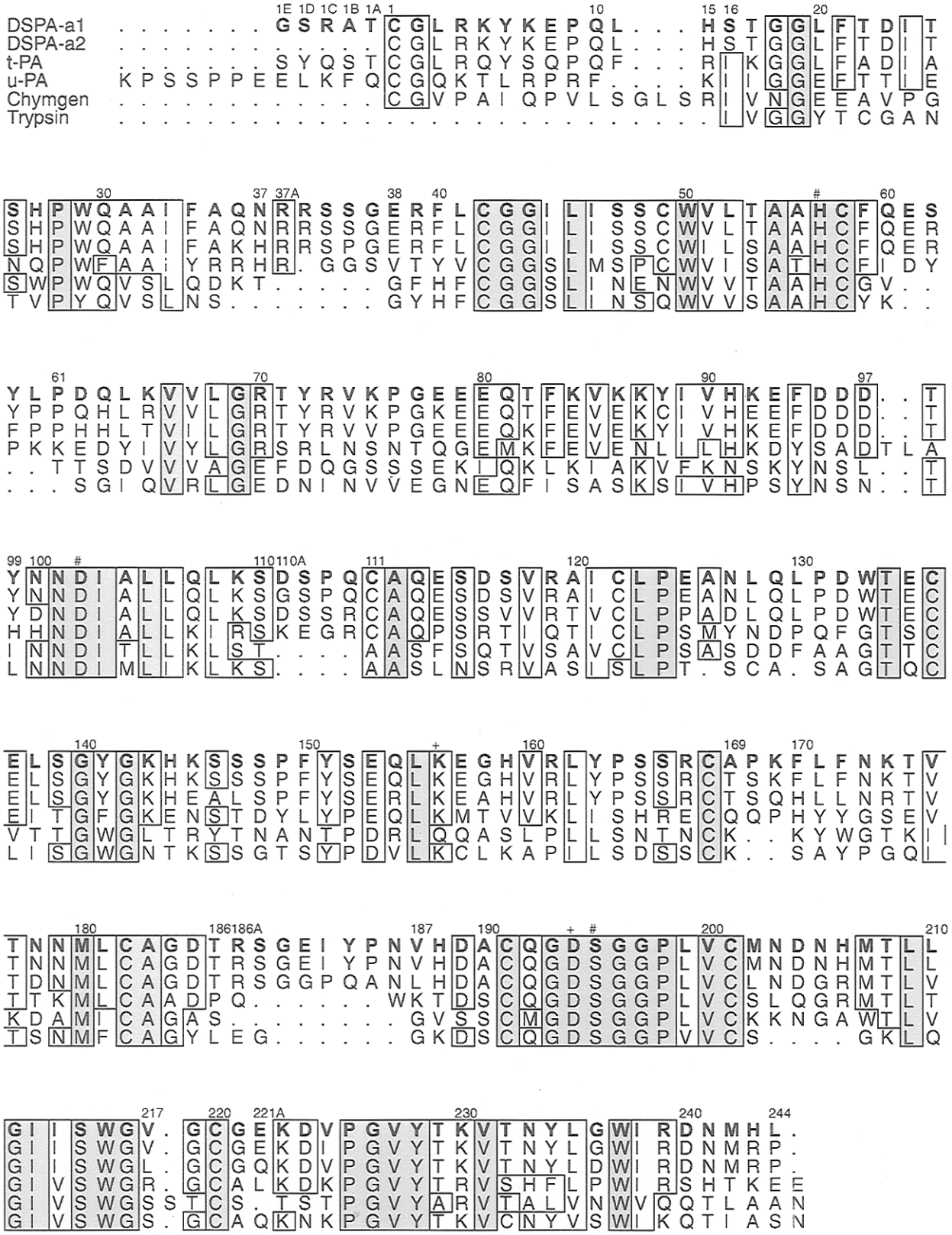

[a] The residues are numbered using the chymotrypsinogen numbering system (for tPA, see ref 2). Conserved regions are marked with boxes, identical regions with gray boxes, and homologous regions with white boxes. The active site residues (His57, Asp102, and Ser195) are shown with hash symbols. The positions of residues Lys156 and Asp194 involved in the formation of the activating salt bridge are indicated by crosses.

solvent-exposed position close to the active site to an internal position at the base of the Ile16 pocket. This reorientation of Asp194 causes a restructuring of four peptide segments (16−19, 142−152, 184−194, and 216−233) surrounding the

specificity pocket, collectively called the activation domain (*10*), to create a functional substrate binding site and oxyanion hole.

Human single-chain (zymogen) tPA is unusual in that it possesses a significant degree of proteolytic activity; in the course of plasminogen activation, it is converted to its more active two-chain form by plasmin. It has been suggested that this single-chain activity might result from specific structural features in the proteolytic domain of tPA that stabilize the enzymatically active form (*2*, *14*−*16*). In contrast, DSPA acts exclusively as a single-chain molecule. In the absence of fibrin, its specific activity toward plasminogen or chromogenic substrates is much lower than that of single-chain human tPA (sc-tPA) (*17*, *18*). In the presence of fibrin polymers, the specific activity of full-length DSPA toward plasminogen is increased by a "fibrin stimulation" factor (ratio of catalytic efficiency in the presence and absence of fibrin) of 102 100. This is considerably higher than that obtained for tPA (550) (*17*), mainly due to a lower catalytic level of DSPA in the absence of fibrin, resulting in similar catalytic efficiencies upon fibrin binding for both enzymes. DSPA also exhibits a higher "fibrin selectivity", defined as the ratio of the catalytic efficiencies in the presence of fibrin and in the presence of fibrinogen, of 12 900 compared with a value of 72 for tPA (*17*). These enormous activity enhancement effects of DSPA are mainly finger domain-dependent; DSPA species lacking the finger domain, such as in β- and γ-DSPA, do not bind to fibrin tightly and are less stimulated.

Nevertheless, the isolated catalytic domain also shows a 30-fold increase in plasminogenolytic activity upon fibrin stimulation (*18*). To improve our current understanding of these activity phenomena, we have crystallized the recombinant catalytic domain of a (ΔFEK)DSPAα_1 variant that contains the catalytic domain of the full-length enzyme and the three N-terminal residues of the signal peptide (−3 to −1, Gly1E, Ser1D, and Arg1C). This structure is compared with two recently elucidated structures of two-chain tPA inhibited with benzamidine [tc-tPA(ba) (*2*)] and with a bisbenzamidine [tc-tPA(bisb) (*1*)]. Both tc-tPA structures display the typical structural features of a cleavage-activated, i.e. mature chymotrypsin-like, serine proteinase in an "enzymatically active conformation". An additional comparison made with the single-chain form of human tPA (sc-tPA), the structure of which has recently been solved (*19*), will help us to identify the features that confer the unique proteolytic activity to single-chain PAs. In this paper, we describe the structure of the DSPAα_1 catalytic domain and try to elucidate the underlying structural mechanism of its catalytic activity and activity enhancement upon fibrin binding.

MATERIALS AND METHODS

Purification and Crystallization. (ΔFEK)DSPAα_1 variant DSPAp was expressed in transfected BHK cells (*20*) and purified by affinity chromatography on ETI-sepharose (*21*). The protein is heterogeneously glycosylated and migrates as a double band on an SDS gel with an apparent molecular mass of 34−36 kDa. DSPAp was reacted with Glu-Gly-Arg-chloromethyl ketone (Bachem) until the remaining activity was below 0.5% of the initial value. Crystals were grown at 20 °C in 10% PEG 8000 and 0.1 M Mes/Tris at pH 8.8−9.2 in sitting drops using the vapor diffusion technique. Fang-shaped crystals grew within 1 week to maximal dimensions of 0.3 × 0.3 × 0.15 mm^3. These crystals belong to the trigonal spacegroup $P3_121$ and have the following cell dimensions: $a = b = 73.86$ Å and $c = 135.19$ Å. They contain one molecule per asymmetric unit, corresponding to a fractional solvent volume of 59% ($V_m = 3.01$ Å^3), taking into account the additional molecular mass due to the glycosylation.

Table 2: Crystal Data and Refinement Parameters for the Catalytic Domain of DSPA

space group	$P3_121$
cell constants	
a	73.86 Å
b	73.86 Å
c	135.19 Å
significant measurements	22 337
independent reflections	9582
limiting resolution	2.9 Å
completeness	97.2% (∞−2.9 Å)
outermost shell	97.9% (3.0−2.9 Å)
R_{merge}[a]	9.2%
outermost shell	40.5% (3.0−2.9 Å)
number of atoms per asymmetric unit	2146
non-hydrogen protein atoms	2084
non-hydrogen inhibitor atoms	25
solvent molecules	37
resolution range	7.0−2.9 Å
reflections used for refinement	8624
completeness (2σ cutoff)	94.2%
outermost shell	94.0% (3.0−2.9 Å)
R value[b]	19.9%
rms standard deviation	
bond lengths	0.009 Å
bond angles	1.702°
RMSB[c]	4.2 Å^2

[a] $R_{merge} = \sum(I-\langle I\rangle)/\sum I$. [b] R value $= \sum(|f_{obs}|-|f_{calc}|)/\sum|f_{obs}|$. [c] RMSB is the rms deviation of the *B*-factor of bonded atoms.

Data Collection, Processing, and Molecular Replacement. Diffraction data up to 2.6 Å resolution were collected on a MAR imaging plate system (MAR Research, Hamburg, Germany) and evaluated using the Mosflm package (*22*) (see Table 2). The structure was solved by Patterson search techniques using the program AMoRe (*23*) with data from 15 to 3.5 Å and the human tc-tPA model [tc-tPA(ba)] (*2*) with the light chain (i.e. residues c1A−c12) omitted. The rotational search yielded one dominant solution with a correlation value of 18.6σ (7.9σ for the next best angle triplet). The translation function corresponding to the highest rotation peak yielded a correlation value of 54.3σ (39.3σ for the next highest peak). Rigid body fitting for these solutions resulted in a correlation value of 61.5 and an *R* value of 36.8%.

Model Building and Refinement. The truncated tc-tPA model used for the Patterson search was subjected to rigid body refinement in X-PLOR (*24*) and subsequent Powell minimization. A 2.9 Å $2f_{obs} - f_{calc}$ map displayed extra density for the backbone of the whole "activation peptide" and for most of the side chains in this segment. Several refinement cycles, consisting of model building using MAIN (*25*), positional minimization, and restrained *B*-factor refinement in latter stages using X-PLOR and the parameters of Engh and Huber (*26*), reduced the *R* value to 19.9%. Thirty-seven water molecules were added to the model. The bonds between the covalent inhibitor and the protein (Ser195Oγ−CF and His57Nδ−CJ) were realized as a patch residue in

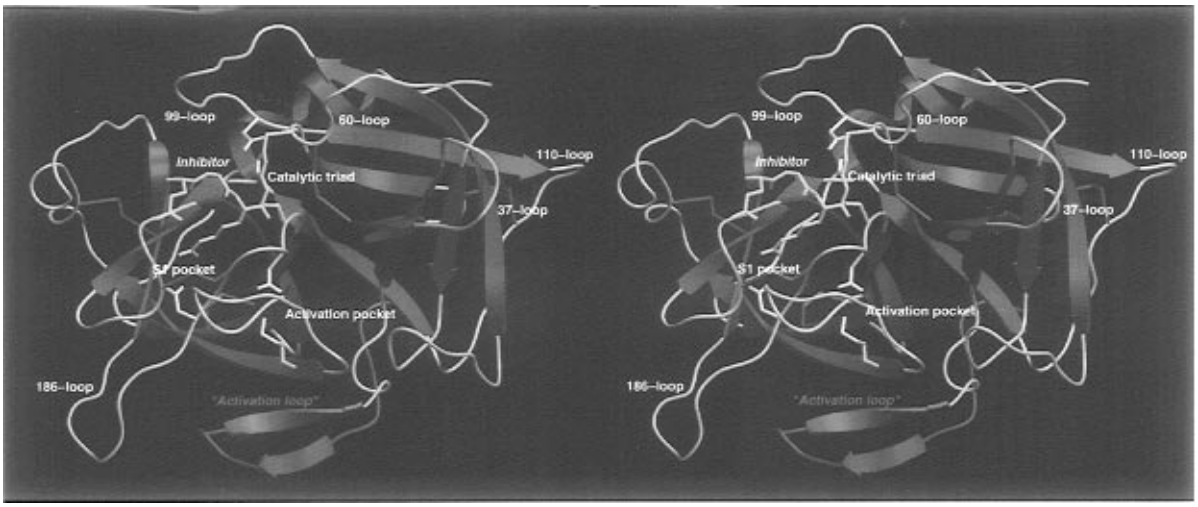

FIGURE 1: Stereo-ribbon plot of the catalytic domain of DSPAα_1 in the standard orientation. The inhibitor Glu-Gly-Arg-chloromethyl ketone, covalently bound to the active site residues His57 and Ser195 (yellow), is shown with green sticks. It forms a salt bridge with Asp189 (yellow) at the bottom of the S1 specificity pocket. The two residues Lys156 and Asp194, conferring stability to the zymogen molecule by forming a salt bridge in the activation pocket, are also shown in yellow. The red ribbon shows the conformation of the N-terminal activation loop. Some loops arranged around the active site are labeled: the mainly disordered 37-loop and the 110-loop to the east; the 186-loop to the southwest is close to the activation loop. For a more detailed description of the function of these surface loops, see ref 2. This figure was prepared using SETOR (*46*).

X-PLOR; values for the target bond lengths and angles were taken from other known structures of serine proteinases with covalently bound chloromethyl ketone inhibitors (*27*−*29*). Very weak angle restraints (about $^1/_{10}$ of the normal values) were chosen for these covalent inhibitor−protein bonds to allow unbiased angle refinement.

Almost all residues of the proteinase domain are defined in the final $2f_{obs} - f_{calc}$ map. The first four residues of the catalytic domain of DSPA, Gly1E, Ser1D, Arg1C, and Ala1B (the signal peptide and one residue of the linker between the kringle domain of full-length DSPA and the catalytic domain), are undefined and therefore not included in the coordinates. Residues making up the segment from His37 to Pro37D and residue Asp110A appear also to be disordered; electron density for five side chains located on the molecular surface is also missing. These residues have been excluded from phasing but are shown in the ribbon plot (Figure 1) and will be given together with the coordinates. The program PROCHECK (*30*) indicates that 73.8% of residues fall within the most favored region of the Ramachandran plot and that no residues are in "disallowed regions". The secondary structure of DSPAp was analyzed using STRIDE (*31*). Crystallographic and final model parameters are given in Table 2.

RESULTS

Overall Structure. The catalytic domain of DSPAα_1 (DSPAp) is a roughly spherical molecule with a radius of 25 Å. It is folded into two six-stranded β-barrels held together by three *trans*-domain straps, one short "intermediate" and one long C-terminal helix, and several surface loops (see Figure 1). The catalytic domain is very similar to other serine proteinases, in particular to the functionally related human tc-tPA (*2*). Optimal superposition of DSPAp with bovine β-trypsin (*32*), bovine chymotrypsin (*33*, *34*), human α-thrombin (*27*, *35*), and the catalytic domains of human urokinase-type plasminogen activator (*28*) and human tc-tPA (*2*) results in 163, 166, 178, 184, and 232 equivalent Cα atoms with rms deviations of 0.74, 0.99, 0.75, 0.81, and 0.51 Å, respectively, using a distance cutoff of 1.5 Å. The topological equivalence of DSPAp with chymotrypsin forms the basis for the chymotrypsinogen numbering of the catalytic domain of DSPAα_1, which has already been introduced for human tc-tPA (*2*). This numbering will be used for DSPAp throughout this paper (see Table 1).

The catalytic domain of DSPAα_1, comprising the 266 residues from Ala1B to Leu244, exhibits two deletions and six insertions totaling 20 additional residues with respect to bovine chymotrypsinogen, like human tPA. One noteworthy three-residue deletion is located in the "activation loop" of DSPA between residues Leu12 and His15. The insertions are found mainly in loop regions, namely around residues Arg37B, Arg60B, Ser110B, Cys168, and Gly186D (in the following referred to as the 37-loop, the 60-loop, the 110-loop, the "intermediate helix", and the 186-loop, respectively; see Figure 1).

Similar to the catalytic domain of human tc-tPA, DSPAp is almost neutral in charge, with 12 arginine, 16 lysine, 16 glutamate, and 15 aspartate residues. Apart from Asp102, Asp194, and Lys156, involved in the catalytic triad and in internal salt bridge formation, respectively (see below), the charged residues are at least partially exposed to the solvent. They are not uniformly distributed along the domain surface but often cluster in positively or negatively charged patches. Similar to that for tPA, a negative potential extends from the active site and the specificity pocket of DSPA (see Figure 2) toward the "north rim" of the active site cleft, where three adjacent residues (Asp95, Asp96, and Asp97) are exposed toward the solvent. A notable positively charged surface patch is observed to the "east" of the active center, including residues of the 37-loop and of the underlying "calcium binding" loop (see below).

Noteworthy Surface Loops. For those unfamiliar with the tPA structure (*2*), a brief description of the DSPAp surface loops that could play a role in interactions with its substrates, inhibitors, and cofactors follows. As for human tPA, most of the surface loops are arranged around the active site and will be addressed in an anticlockwise manner (see Figure

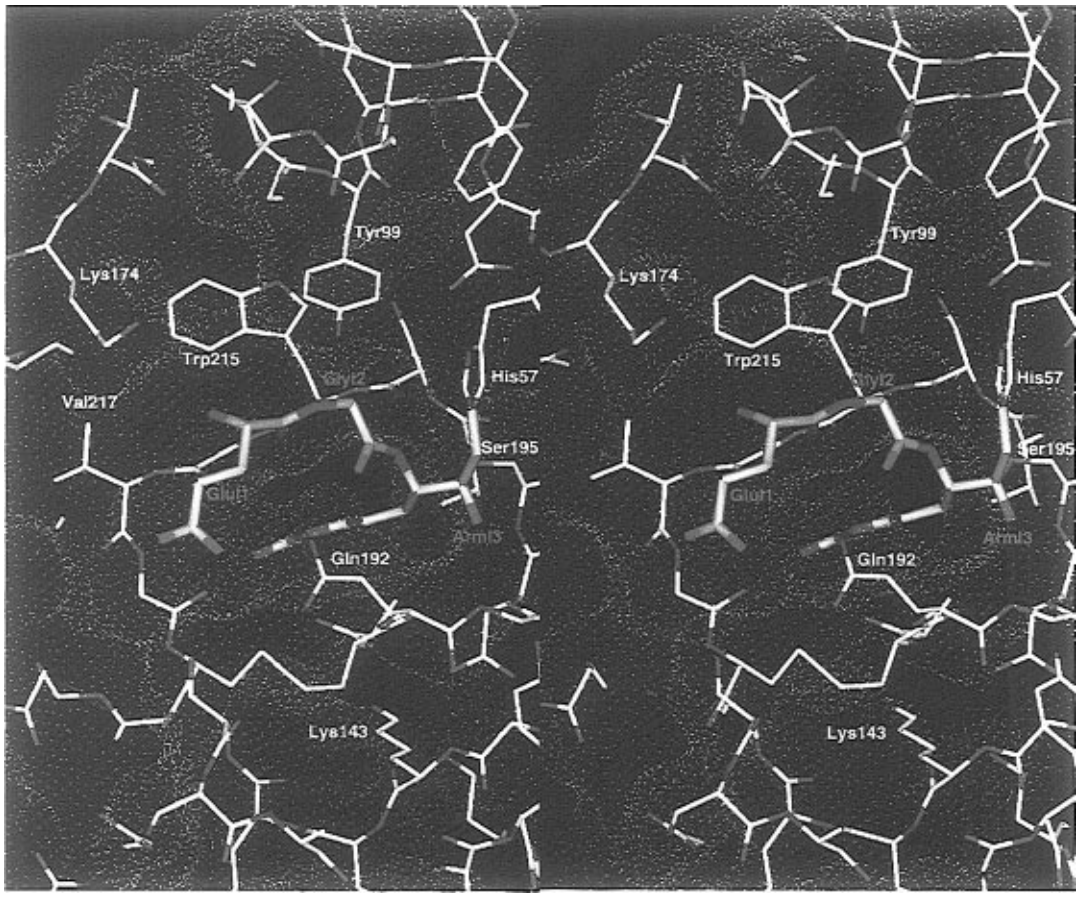

FIGURE 2: Stereoplot of the active site environment of the catalytic domain of DSPAα_1 in the same orientation as Figure 1. The covalently bound inhibitor is shown in orange. The inhibitor backbone, kinked at P2−GlyI2, juxtaposes DSPA segment Ser214−Val217 via formation of a twisted antiparallel β-sheet. Its Arm group forms covalent bonds with Oγ of Ser195 and Nϵ_2 of His57 and a salt bridge with Asp189 (not shown) at the bottom of the S1 specificity pocket. Its GlyI2 group is close to the impending Tyr99 of the 99-loop, probably resulting in unfavorable interactions. The GluI1 carboxylate group makes polar hydrogen bond interactions with Gly219N and the carboxamide nitrogen of Gln192. The basic side chain of Lys174 restricting the S4 pocket to its western side is not involved in stabilizing interactions with the inhibitor.

1). For a more detailed discussion, see the description of the catalytic domain of human tPA (*2*).

To the east of the active site, the 37-loop projects away from the molecular surface near the active site cleft. As in tPA, the six peripheral residues Asn37−Gly37D are disordered despite their potential stabilization by a neighboring molecule. The interrupted density would nevertheless allow placement of a quite open hairpin loop with a conformation like that suggested for tc-tPA(ba), with the side chains of Arg37A and Arg37B extending away from the active site cleft. The almost strict conservation of the Arg/Lys37A-Arg37B-Ser37C-X37D-Gly37E-Glu38-Arg39 pattern in all tPAs sequenced so far (bovine, human, rat, and mouse tPAs; several vampire bat PAs) suggests that this loop has an important role. Indeed, this loop has been shown to be of fundamental importance for the interaction of tPA with its natural inhibitor PAI-1 (*36*, *37*) as well as for the fibrin specificity and stimulation of plasminogenolytic activity for tPA variants (*38*, *39*). Disorder of this loop, which we have now observed for human sc-tPA, human tc-tPA, and DSPAp in four different crystal forms, seems to be an inherent property of all tPAs and might be necessary for its function.

To the north and directly adjacent to the 37-loop is the 60-loop, which extends along the molecular body with a conformation almost identical with human tPA. Residue Glu60A is not properly defined in the electron density but should extend with its side chain toward the defined guanidinium group of Arg39 as in tPA (*2*). This 60-loop is more negatively charged than that in tPA (see Table 1), and the change from Pro60D to Leu60D might render it more flexible. The nearby side chain of Tyr88 is found in a shallow surface depression similar to tPA; the equivalent Cys side chain in the DSPAα_1 variant must be accommodated in a similar manner, i.e. should be partially accessible to bulk solvent.

Identical with human tPA, the β-hairpin loop from Lys92 to Asn100 protrudes from the north rim of the active site cleft toward the active site (see Figure 2). The amino acid sequences of human tPA and DSPA are identical and conserved in this region, apart from residue 100. At its most exposed part, the acidic side chains of Asp95, Asp96, and Asp97 project away from the active site cleft; that together with Glu93 forms a rather acidic surface patch. This acidic region can serve as an anchoring point for positively charged moieties of inhibitors, as seen in the structure of human tc-tPA(bisb) (*1*). The side chain of Tyr99 points toward the active site parallel to Trp215, where it blocks the S2 subsite (see Figure 2).

Lys174 of the adjacent loop extends toward the substrate binding site (see Figure 2). The fully defined side chain of the preceding Asn173, which (as in tPA) seems to be the single carbohydrate linkage site of the DSPA catalytic domain (*40*), extends away from the active site cleft; thus, a bound oligosaccharide should not grossly interfere with

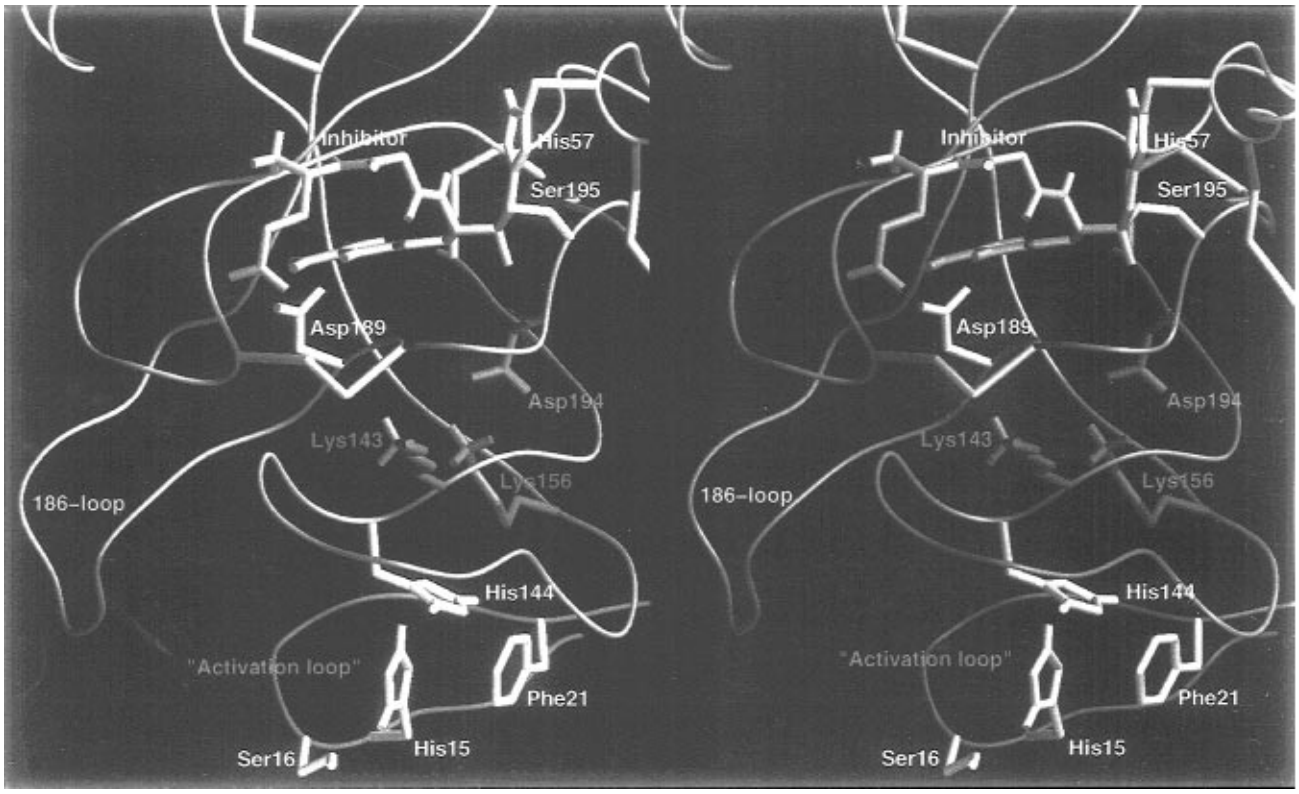

FIGURE 3: Stereoplot of the activation domain environment of DSPAα_1 involving residues of the activation pocket, the activation loop, and Lys156. Lys156 (blue) stabilizes the active conformation of DSPAα_1 via formation of a salt bridge with Asp194 (red). The strength of this interaction is presumably increased by the concerted solvent shielding effect of the activation loop (red) and of the hydrophobic residues Phe21 and His144 (yellow), which are conserved among the DSPAs and tissue-type plasminogen activators. Lysine 143, which was considered a potential activator of human sc-tPA (*47*), is also shown (blue).

productively bound substrates (see also ref 2). Although the crystallized enzyme is glycosylated (see Materials and Methods), no additional density was observed for a carbohydrate. Despite their different sequences, the preceding residues Ala169, Pro169A, Lys169B, and Phe170 are accommodated in a conformation very similar to that in tPA.

To the southwest of the active site cleft of DSPAp is the 186-loop (see Figure 1), whose seven- to eight-residue insertion from Arg186A to Asn186H is characteristic of tPAs and DSPAs. In contrast to the tc-tPA(ba) structure (*2*), this loop is well-defined in DSPA. Similar to tc-tPA(bisb) (*1*), it encircles the extended side chain of the conserved residue Lys222, which hydrogen bonds to the carbonyls of Gly186C and Tyr186F via its ϵ-ammonium group. This loop appears to fold autonomously, making contact with other loops only through the Tyr186F side chain with Gly19 of the adjacent activation loop (see below). Five residues are exchanged in this loop with respect to human tPA, rendering it more polar in DSPA.

The "autolysis loop" Tyr141−Tyr151 forms the "southern rim" of the active site cleft with a conformation similar to that observed in tc-tPA (see Figures 1 and 2). It forms part of the activation domain, interacting directly with the activation loop (see below). The three residues Lys145, Ser146, and Ser147 differ from their counterparts in tPA, significantly altering the environment of the activation loop. As in human tPA, the side chain of Tyr151 extends into the S2′ subsite.

The 70−80-loop adjacent to the autolysis loop and behind the 37-loop (see Figure 1) is topologically similar to the "calcium binding loop" of trypsin and of related proteinases (*32*). As in human tPA, the "calcium site" of DSPA is occupied by the guanidinium group of Arg70, with its nitrogen atoms in hydrogen and/or ionic bond distance with respect to the carbonyl oxygen atoms of Tyr72 and Arg73 and to the carboxylate group of Glu80. This is reminiscent of the equivalent loops in thrombin (*27*), porcine pancreatic kallikrein, and leukocyte elastase, where likewise the distal basic side chains of Lys70, Arg70, and Arg80 replace the calcium ion, respectively, conferring these serine proteinases a stability independent of ambient calcium levels.

Almost opposite to the active site cleft of DSPA, a four-residue insertion loop (Asp110A, Ser110B, Pro110C, and Gln110D) bulges away from the molecular surface. Although two residues are exchanged relative to human tPA, all Cα positions are almost identical. Despite its short length, this handle-shaped loop appears to possess considerable mobility in plasminogen activators, fixed to the main molecular body through the disulfide bridge Cys49−Cys111 characteristic of tPA, uPA, and DSPA.

N-Terminal Segment and Activation Loop. The N-terminal segment begins on the domain surface almost opposite the active site cleft, covalently clamped to the main molecular body via disulfide Cys1−Cys122. It is comprised of the three signal peptide residues Gly1E, Ser1D, and Arg1C, the two residues Ala1B and Thr1A which link the kringle domain of full-length DSPA to the catalytic domain, and the initial part of the activation peptide (in analogy to the other serine proteinases, terms such as activation peptide and activation loop are maintained).

Residues Cys1−His15 follow the molecular surface in an almost extended conformation (see Figure 3). Peptide

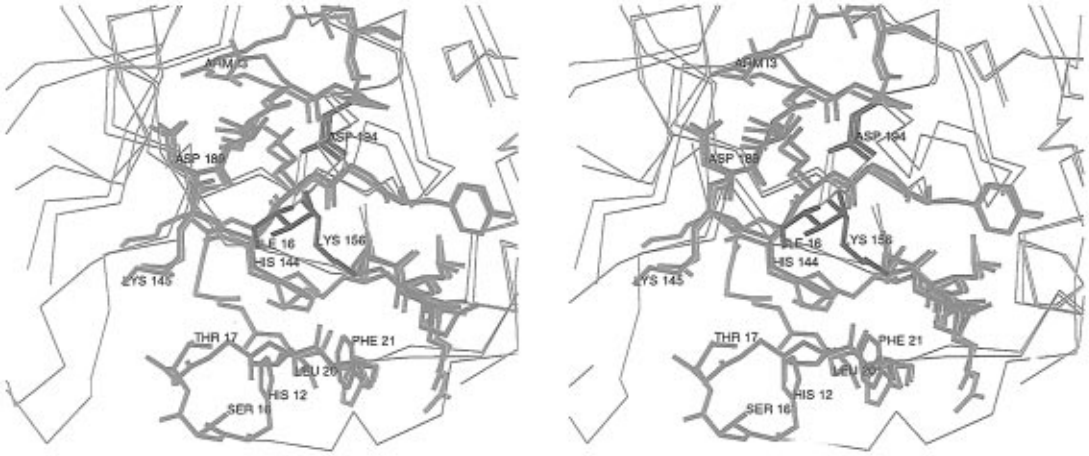

FIGURE 4: Superposition of the activation domains of DSPAα_1 (orange) and tc-tPA (blue) (*1*). This figure shows the difference in the activation mechanism of the two plasminogen activators. In DSPAα_1 the active conformation is stabilized by the salt bridge between Asp194 and Lys156 in the activation pocket. The environment of the activation pocket contributes stability to this salt bridge. The hydrophobic residues Phe21 and His144 partially shield the activation pocket from solvent (see also Figure 3). In the two-chain form, the aliphatic part of the Lys156 side chain is packed between side chains of Ile16, His144, and Phe21, while its distal ammonium group is anchored via hydrogen bonds to Ile16O and Gly18O; the first three N-terminal residues Ile16, Lys17, and Gly18 of the B-chain are part of a three-stranded β-sheet including the segments Lys143-His144 and Asp189-Ala190 (*2*).

segment Gln10−Phe21 is accommodated on the molecular surface as an extended β-hairpin activation loop, with four main chain hydrogen bonds (Gln10N···Phe21O, Gln10O···Phe21N, His15N···Gly19O, and His15O···Gly18N) formed between the antiparallel strands. Segment His15-Ser16-Thr17-Gly18 forms an almost regular 1,4-tight turn that stands slightly away from the surface but is well defined by density. The following peptide group Gly18-Gly19 bulges out of the exiting strand, interrupting the otherwise regular two-strand ladder.

The equivalent activation loop of sc-tPA has an identical number of residues; due to a single residue insertion Phe11 and a single residue deletion before Ala22 (*19*), it forms a kinked β-hairpin loop, with its Ile16-Lys17-Gly18-Gly19 turn located at a different surface site. Thus, the DSPA and the tPA turns are sequentially shifted from one another by one residue, with His15-Ser16 of DSPA equivalent by sequence, but Leu11-His15 by topology to the tPA scissile bond from Arg15 to Ile16. Neither of these two bonds in DSPA should be susceptible to serine proteinases of trypsin or plasmin-like specificity.

Activation Site and the Ile16 Pocket. The activation loop forms a lid over a surface groove that separates three fixed buried water molecules from the bulk solvent. This groove is bounded by the extended activation loop segment His12−Phe21 and the contiguous surface presented by the side chains of His144, Phe21, and His15 to the south, by the five residues from Tyr186F to His188 to the west, by main chain segment Asp189−Gly193 and disulfide bridge 191−220 to the north, and by the curled main chain segments Gly140−His144 and Ser152−Lys156 to the east (see Figure 3). Most noteworthy, the side chain of Lys156 in the center of this groove points inward toward the Ile16 pocket as a result of a χ_1 angle of 60°. Its distal ammonium group is engaged in a buried salt bridge with the carboxylate group of Asp194, which is found in its "internal active" conformation, i.e. with its side chain rotated inward and approaching the Ile16 pocket. The ϵ-ammonium group of Lys156 also forms a hydrogen bond to the nearby carbonyl group of Lys143.

In activated tc-tPA (see Figure 4), main chain segments Arg154−Gly158 and 143−145 are arranged similarly around the Ile16 pocket. In contrast to that of DSPA, however, the χ_1 angle of −60° causes the Lys156 side chain to extend away from the molecular surface; it is the free α-ammonium group of the N-terminal segment Ile16-Lys17-Gly18-Gly19 that forms a salt bridge to Asp194. In the activated tc-tPA conformation, the aliphatic portion of Lys156 is framed by the side chains of His144 and Phe21 (conserved among plasminogen activators), and Nζ forms hydrogen bonds to the carbonyl groups of Ile16 and Gly18. Due to the conformation and location of the activation loop, this latter stabilizing interaction could not take place in DSPA. The external conformation of Lys156 thus appears to be disfavored energetically, shifting the equilibrium toward an internal location and thereby stabilizing the activating salt bridge formed with Asp194.

The activation loop contacts the 186-loop through Gly18···Tyr186F. The two loops form a contiguous surface cap over the activation domain. This surface cap embraces a shallow surface depression which carries a number of conserved charged residues: Glu135, His159, Arg161, Asp185, and Arg186A (toward the back in Figure 1; see Figure 3). It has been suggested that the equivalent residues in tPA are involved in fibrin stimulation (*39*); indeed, such a "fibrin attachment site" would be an ideal cofactor binding site for influencing the inactive−active equilibrium of tPA and DSPA (see below).

Active Site Cleft. In agreement with the internal active conformation of Asp194, the active site and the adjacent substrate binding subsites of DSPAp are virtually identical with their activated tc-tPA counterparts. Main chain segment Cys191−Asp194 is turned outward, opening the specificity pocket and positioning Gly193 correctly to form a functional oxyanion hole (see Figure 2). The specificity pocket of the DSPAp−inhibitor complex, bordered by segment Ile213−Cys220 (the entrance frame), Asp189−Ser195 (the base), Pro225−Thr229 (the back of the pocket), and the disulfide bridge Cys191−Cys220 (closing toward the south), is virtually identical with that of activated tc-tPA. Due to the lack of a polar residue at position 190, DSPA, like tPA, is

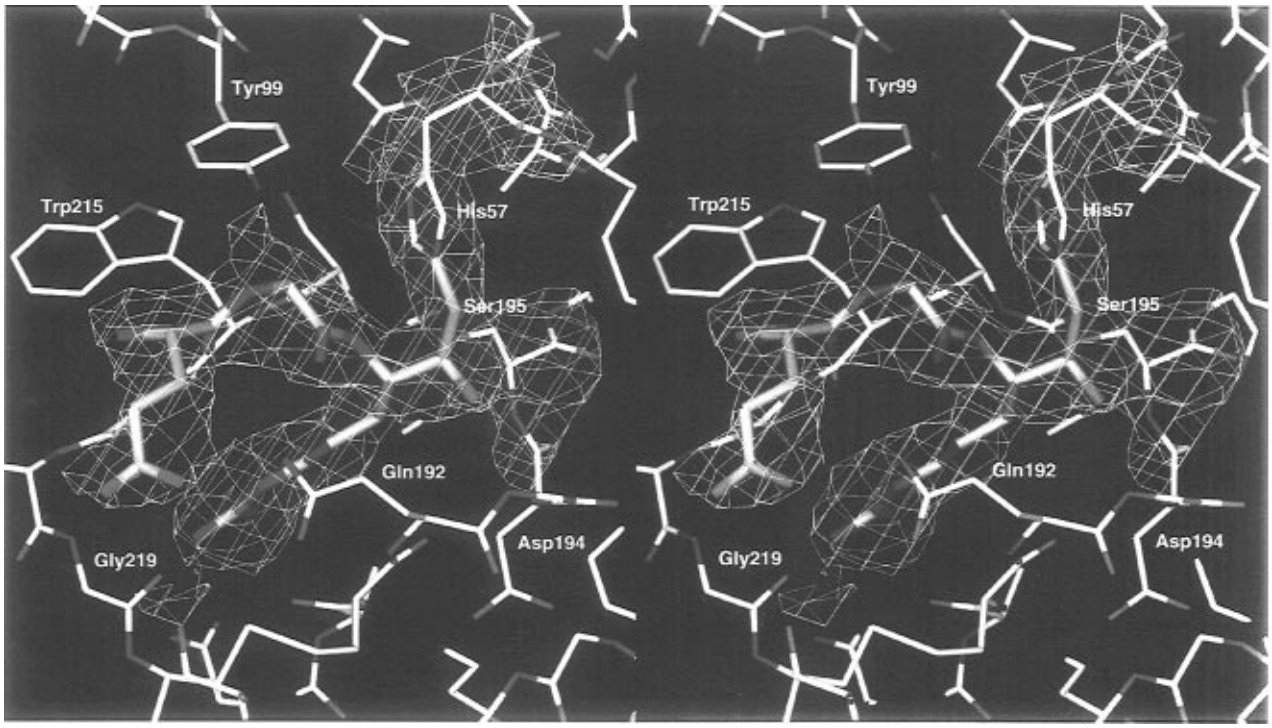

FIGURE 5: Glu-Gly-Arg-chloromethyl ketone inhibitor (orange) and part of the active site of sc-tPA (yellow) superimposed on the final $2f_{obs} - f_{calc}$ electron density. Contoured at 0.9σ, oriented as in Figure 1. This figure was prepared using Main (*25*).

expected to have a preference for P1 Arg residues over Lys. The S2 site is restricted in size due to the impending Tyr99 phenolic group, and the S3/S4 subsites extend over the Trp215 indole moiety, bounded by the Lys174 side chain and the 174−175 peptide bond to the west, the side chains of Thr175 and Thr98 to the north, and the carbonyl oxygens 97O and 98O and the Tyr99 phenolic side chain to the east (see Figure 2).

Except for a few small conformational differences originating from the covalent interactions with the inhibitor, the residues of the active site triad, Ser195, His57, and Asp102, are in the characteristic active conformation illustrated by the tc-tPA structures. The active site cleft is similar in shape, bordered to the north by the bulging 174-loop, the protruding 99-loop, the initial part of the 60-loop, and the Phe40 and Leu41 side chains of the 37-loop and to the south by the side chains of the bulged autolysis loop (see Figure 2). As in tPA, several polar/charged residues protrude into this cleft (in particular Lys174, Asp96, Asp97, Tyr99, Glu60, and Glu60A), which is hydrophobic at its base to the west (Phe172 and Val217), but more polar in its central and eastern part. In general, the active site cleft of DSPA seems to be slightly more polar, due to a few changes from hydrophobic to polar residues in its western (Gln221A → Glu and Ala146 → Ser) and eastern part (Val75 → Lys and Pro37D → Ser).

Inhibitor Binding. As shown in Figure 5, the H-L-Glu-Gly-Arg-methylene inhibitor moiety bound to the substrate binding site is fully defined by electron density. The inhibitor makes many contacts with its target proteinase and is not involved in any direct interactions with symmetry-related complexes. The continuous density from the carbonyl carbon atom and the methylene group of the inhibitor P1 Arg-methylene (ArmI3) residue to Ser195Oγ and His57Nϵ_2 of DSPA indicates covalent bond formation, and the density distribution around the P1 carbonyl carbon is in agreement with the expected tetrahedral geometry of the hemiketal formed (see Figure 5). The inhibitor backbone, kinked at P2−GlyI2, juxtaposes DSPA segment Ser214−Val217 via formation of a twisted antiparallel β-sheet. Favorable inter-main chain hydrogen bonds are made between ArmI3N and Ser214O and between GluI1O and Gly216N. The α-ammonium group of the inhibitor residue GluI1 is shifted away slightly from an optimal position for a hydrogen bond with Gly216O (3.3 Å). This shift might be caused by the polar hydrogen bond interactions of the GluI1 carboxylate group made with Gly219N (3.1 Å) and the carboxamide nitrogen of Gln192 (3.6 Å).

The side chain of the P1 residue, ArmI3, extends in a zigzag like manner into the DSPA specificity pocket, where it is sandwiched between the main chain segments of Trp215-Gly216 and Cys191-Gln192. Its distal guanidinium group is engaged in a symmetric salt bridge with the carboxylate of Asp189 at the bottom of the pocket (3.3 and 3.1 Å), and in an N···O hydrogen bond with the carbonyl oxygen of Gly219 (3.3 Å). The electron density gives no indication of an internal water molecule, as normally observed toward the back wall of the pocket (*27*). The gap between the side chain and the pocket wall remains, probably reflecting the relatively hydrophobic character of the DSPA pocket.

Main chain atoms N and Cα of the preceding inhibitor residue, GlyI2, are in close contact with the distal part of the phenolic side chain of Tyr99; GlyI2N makes a weak hydrogen bond to Tyr99Oη. The Tyr99 phenolic ring is parallel to the Trp215 indole moiety, perpendicular to that observed in tc-tPA(ba) and tc-tPA(bisb). The Tyr99 orientation in the DSPA complex seems to be determined by the more favorable steric interactions with the inhibitor main chain. Side chains of larger P2 residues would collide with the phenolic group, requiring the displacement of one group or another out of this site, in agreement with the preference of tPAs for Gly residues at P2. The side chain of the P3

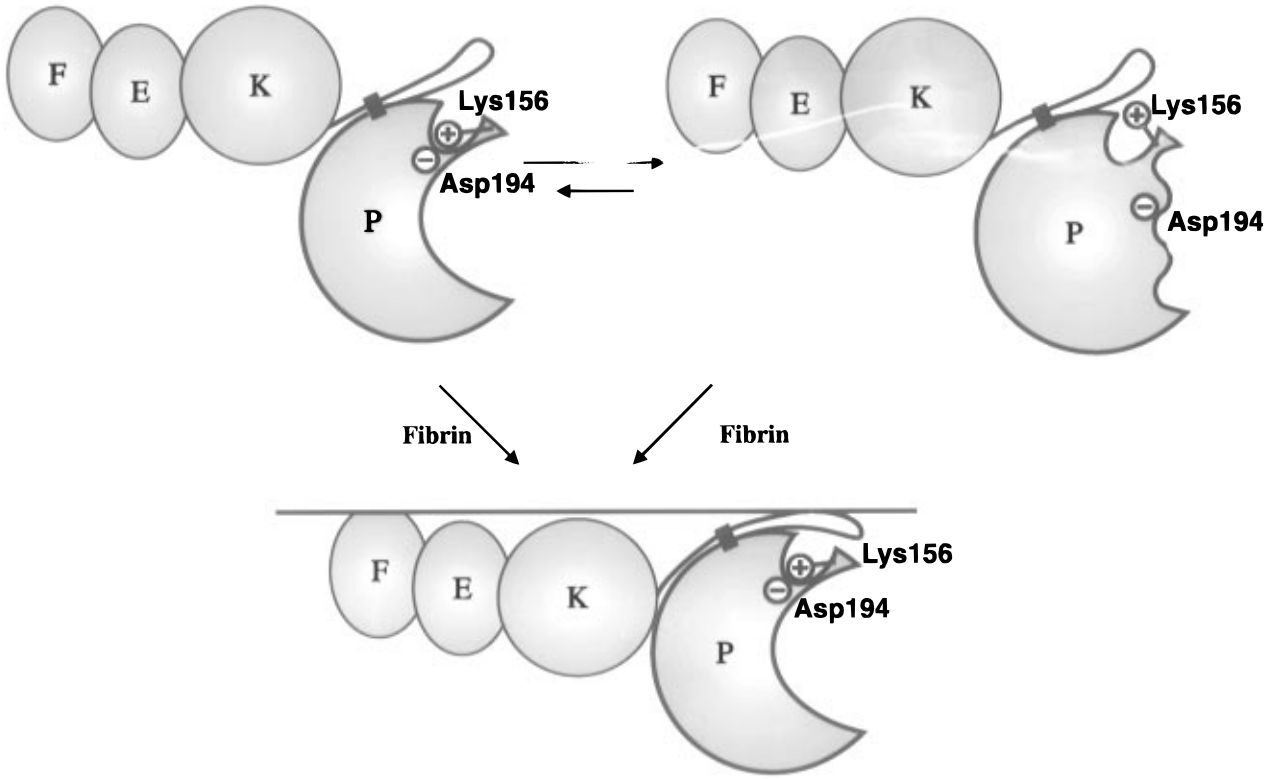

FIGURE 6: Schematic representation of the full-length DSPA molecule showing the putative equilibrium between the enzymatically active and the inactive states. In the enzymatically active form, Lys156 and Asp194 form a stabilizing salt bridge. This salt bridge does not exist in the enzymatically inactive form, leading to a disordered activation domain. The equilibrium between the two forms is thought to lean toward the enzymatically inactive form. Binding to fibrin, largely mediated via the finger domain, induces the shift to the enzymatically active state. In contrast to human tPA, the kringle of DSPA does not possess a lysine binding site and does not contribute to the binding (DSPAγ, consisting of the catalytic domain and the kringle, does not bind to fibrin). Weak interactions between the fibrin template and the catalytic domain are postulated. The activation loop might approach the molecular body of the catalytic domain upon fibrin binding, closing the activation pocket from solvent and thereby stabilizing the interaction between Lys156 and Asp194.

residue Glu points away from the molecular surface due to its L configuration (see Figure 2), forming a hydrogen bond to the amide nitrogen of Gly219.

DISCUSSION

As anticipated from the high sequence homology, the spatial structure of the DSPA catalytic domain is very similar to that of the activated form of tPA, tc-tPA. DSPAp therefore exhibits structural elements that are probably characteristic of tPA catalytic domains, such as the partially flexible handle-like 110 (or plasminogen activator)-loop and its clamping disulfide bridge Cys49−Cys110, the exposed basic and highly flexible 37-loop presumed to be involved in PAI-1 binding, and the extremely exposed 186-insertion loop.

Due to the enzymatically active conformation of the DSPA complex, however, the similarity with the two-chain form of tPA also extends to the substrate binding site. In particular, the active site S1 specificity pocket and subsites S2 and S3/S4 as well as S1′ and S2′ are virtually identical. Thus, the substrate specificity of DSPA is also presumably very similar to that of the more intensively studied human tPA.

Remarkable structural differences with respect to the tc-tPA structure are observed only in the vicinity of the activation loop and the Ile16 pocket. A comparison with the sc form of tPA recently elucidated in our laboratory (*19*) shows a close similarity, yet noteworthy differences between the two single-chain molecules are seen in this region, which might confer the lower basic activity and larger stimulation enhancement of DSPA upon fibrin binding.

This structure fits well into the concept of two structurally and functionally distinct molecular forms for single-chain chymotrypsin-like serine proteinases (*11*, *14*). These form an enzymatically inactive form with a disordered or malformed activation domain and an external Asp194 and an enzymatically active form with a folded activation domain and an internal Asp194. An equilibrium exists between the two forms which for most serine proteinases lies heavily toward the inactive form [e.g. the equilibrium constant for bovine trypsinogen has been estimated to be 10^7 (*11*)]. The equilibrium can be influenced by stabilization/destabilization of one inactive form or the other through either intramolecular or intermolecular ("cofactor") interactions. The active form is stabilized by the endogenous Ile/Val16 N terminus revealed upon activation cleavage, but may also be induced by exogenous Ile-Val dipeptides (*11*) or high-affinity inhibitor binding (*11*, *41*). In contrast, the zymogen form may be stabilized via the "zymogen triad" Asp194-His40-Ser32 in the pancreatic serine proteinases (*8*, *12*) and tPA mutants (*15*).

The lack of an activation cleavage site in DSPA precludes the "normal" switch that triggers an active conformation. Instead, the two-state equilibrium is shifted toward the active single-chain conformation by the suitably placed side chain of Lys156. The ϵ-amino function of Lys156 substitutes for the free amino-terminal Ile16 of cleavage-activated serine proteinases, forming a salt bridge with the side chain of

Asp194, thereby forcing the internal conformation of the latter and concomitant creation of substrate binding subsites. The orientation of the Lys156 side chain is presumably influenced by the surrounding residues; the side chains of Phe21 and His144 (*19*, *42*) and the irregular bulge of the activation loop at Gly18-Gly19 may help establish this conformation and at the same time remove potential alternative hydrogen bonding partners for Lys156. Indeed, apart from DSPA and tPA, all serine proteinases with a Lys residue at position 156 have hydrogen bond acceptors in the vicinity which prevent Lys156−Asp194 salt bridge formation and thus contribute to the stabilization of the inactive zymogen conformation (*19*, *43*). Mutagenesis studies on human tPA confirm this important role; Lys156 → Tyr mutants indeed have lower single-chain activity than the wild-type enzyme and have therefore a substantially enhanced zymogenicity (*43*).

The suitable positioning of Lys156 in DPSA is insufficient to drive the conformation equilibrium fully to the enzymatically active form, as DSPA is virtually inactive in the absence of fibrin, in contrast to sc-tPA. The anomalous reactivity of DSPA toward specific peptidyl chloromethyl ketones [in contrast to e.g. sc-uPA (*44*)], on the other hand, shows that a significant population of "active" DSPA molecules must exist. Peptidyl chloromethyl ketones will only form covalent bonds to Ser195 and His57 if the subsites S1−S3/S4 and the oxyanion hole are arranged to accept the docking peptide moiety (see ref 45 for references). In the course of covalent bond formation, the disturbed conformational equilibrium will be continuously re-established, resulting in the complete transformation of inhibited DSPA toward the active conformation, as observed in these DSPA crystals.

Unligated DSPA seems to attain full activity only in the presence of fibrin, a phenomenon associated to a large extent with the N-terminal finger domain (*17*). A considerable part of this stimulation effect can be attributed to assembling, i.e. the suitable arrangement of proteinase and substrate on the cofactor template, forcing the active site of the DSPA catalytic domain and the activation site of plasminogen together in a productive orientation (see Figure 6). The considerable increase in amidolytic activity (i.e. cleavage of small chromogenic substrates) of both full-length DSPA and the catalytic domain upon fibrin binding, however, is an indication of additional allosteric effects exerted on the active center upon fibrin binding. The changed stimulation properties of certain alanine scanning mutants of tPA (*39*) suggest that several residues on the tPA catalytic domain surface are involved in fibrin stimulation, in particular those forming the fibrin attachment site. This attachment site consists of three segments centered at Glu135, His156−Arg161, and Arg185-Arg186A, i.e. residues situated in the neighborhood of the activation loop. A chimeric human tPA containing the sequence of the homologous DSPA 186-loop was 4 times more fibrin specific than wild-type tPA (*38*). A human tPA mutant with a five-residue deletion showed significantly reduced plasminogenolytic activity in the presence of fibrinogen; however, this variant maintained normal stimulation behavior toward fibrin (*38*).

We hypothesize that the finger domain-mediated anchorage of DSPA to fibrin results in the juxtaposition of specific surface features of the fibrin template and the DSPA catalytic domain. As the fibrin attachment site of tPA (and by analogy DSPA) includes the 186-loop and the activation loop, it is conceivable that fibrin binding induces an organization of the activation domain as seen in the present structure. Through stabilization of the Lys156−Asp194 salt bridge, the zymogen equilibrium is shifted fully toward the active conformation, generating the observed high plasminogenolytic activity of fibrin-bound DSPA.

Through the lack of an activation site, DSPA represents an extreme variation on the theme of serine proteinase activity, which ranges from the almost wholly zymogenic activity of tPA, through the partial activity of DSPA, the normal inactive zymogens of the pancreatic serine proteinases, to the cofactor-stimulated factor Xa and the virtually inactive factor IXa that only achieves full activity in its activated form in the presence of its cofactor, factor VIIIa. Nature has used these varying degrees of activity to allow precise modulation and regulation of proteolytic pathways, notably those of hemostasis. For that of the vampire bat, the lack of activity in the absence of fibrin prevents the digestion of endogenous saliva proteins and locates the activation of the victim's plasma plasminogen only to the bleeding wound where fibrin is constantly formed. This has an advantage in that inflammatory processes are reduced, allowing the bat to feed while the victim sleeps (witness the fate of mosquitoes that cause inflammation and pain). The vampire bat has developed a proteinase that works as well as endogenous tc-tPA, but that in contrast to the latter loses activity on dissociation from fibrin, so that it cannot interfere with other tPA functions.

REFERENCES

1. Renatus, M., Bode, W., Huber, R., Stürzebecher, J., Prasa, D., Fischer, S., Kohnert, U., and Stubbs, M. T. (1997) *J. Biol. Chem. 272*, 21713−21719.
2. Lamba, D., Bauer, M., Huber, R., Fischer, S., Rudolph, R., Kohnert, U., and Bode, W. (1996) *J. Mol. Biol. 258*, 117−135.
3. Markwardt, F. (1994) *Pharmazie 49*, 313−316.
4. Hawkey, C. (1966) *Nature 211*, 434−435.
5. Apitz-Castro, R., Béguin, S., Tablante, A., Bartoli, F., Holt, J. C., and Hemker, H. C. (1995) *Thromb. Haemostasis 73*, 94−100.
6. Krätzschmar, J., Haendler, B., Langer, G., Boidol, W., Bringmann, P., Alagon, A., Donner, P., and Schleuning, W.-D. (1991) *Gene 105*, 229−237.
7. Gardell, S. J., Duong, L. T., Diehl, R. E., York, J. D., Hare, T. R., Register, R. B., Jacobs, J. W., Dixon, R. A. F., and Friedman, P. A. (1989) *J. Biol. Chem. 264*, 17947−17952.
8. Freer, S. T., Kraut, J., Robertus, J. D., Wright, H. T., and Xuong, N. H. (1970) *Biochemistry 9*, 1997−2009.
9. Fehlhammer, H., Bode, W., and Huber, R. (1977) *J. Mol. Biol. 111*, 415−438.
10. Bode, W., and Huber, R. (1978) *FEBS Lett. 90*, 265−269.
11. Bode, W. (1979) *J. Mol. Biol. 127*, 357−374.
12. Wang, D., Bode, W., and Huber, R. (1985) *J. Mol. Biol. 185*, 595−624.
13. Shotton, D. M., and Hartley, B. S. (1970) *Nature 225*, 802−806.
14. Nienaber, V. L., Young, S. L., Birktoft, J. J., Higgins, D. L., and Berliner, L. J. (1992) *Biochemistry 31*, 3852−3861.
15. Madison, E. L., Kobe, A., Gething, M. J., Sambrook, J. F., and Goldsmith, E. J. (1993) *Science 262*, 419−421.
16. Tachias, K., and Madison, E. L. (1995) *J. Biol. Chem. 270*, 18319−18322.
17. Bringmann, P., Gruber, D., Liese, A., Toschi, L., Krätzschmar, J., Schleuning, W.-D., and Donner, P. (1995) *J. Biol. Chem. 270*, 25596−25603.
18. Toschi, L., Bringmann, P., Petri, T., Donner, P., and Schleuning, W.-D. (1997) *Eur. J. Biochem.* (submitted for publication).

19. Renatus, M., Stubbs, M. T., Engh, R. A., Huber, R., Fischer, S., Kohnert, U., and Bode, W. (1997) *EMBO J. 16*, 4797−4805.
20. Wirth, M., Bode, J., Zettlmeissl, G., and Hauser, H. (1988) *Gene 73*, 419−426.
21. Heussen, C., Joubert, F., and Dowdle, E. B. (1984) *J. Biol. Chem. 259*, 11635−11638.
22. Leslie, A. G. W. (1994) *Mosflm User Guide, Mosflm verion 5.20*, MRC Laboratory of Molecular Biology, Cambridge, U.K.
23. Navaza, J. (1994) *Acta Crystallogr. A 50*, 157−163.
24. Brünger, A. (1992) *X-PLOR (Version 3.1). A System for X-ray Crystallography and NMR*, Yale University Press, New Haven, CT.
25. Turk, D. (1992) Weiterentwicklung eines Programmes für Molekülgraphik und Elektronendichte-Manipulation und seine Anwendung auf verschiedene Protein-Strukturaufklärungen, Ph.D. Thesis, Technische Universität München, München, Germany.
26. Engh, R. A., and Huber, R. (1991) *Acta Crystallogr. A 47*, 392−400.
27. Bode, W., Turk, D., and Karshikov, A. (1992) *Protein Sci. 1*, 426−471.
28. Spraggon, G., Phillips, C., Novak, U. K., Ponting, C. P., Saunders, D., Dobson, C. M., Stuart, D. I., and Jones, E. Y. (1995) *Structure 3*, 681−691.
29. Brandstetter, H., Bauer, M., Huber, R., Lollar, P., and Bode, W. (1995) *Proc. Natl. Acad. Sci. U.S.A. 92*, 9796−9800.
30. Laskowski, R. A., MacArthur, M. W., Moss, S. D., and Thorton, J. M. (1993) *J. Appl. Crystallogr. 26*, 283−291.
31. Frishman, D., and Argos, P. (1995) *Proteins: Struct., Funct., Genet. 23*, 566−579.
32. Bode, W., and Schwager, P. (1975) *J. Mol. Biol. 98*, 693−717.
33. Birktoft, J. J., and Blow, D. M. (1972) *J. Mol. Biol. 68*, 187−240.
34. Blevins, R. A., and Tulinsky, A. (1985) *J. Biol. Chem. 260*, 4264−4275.
35. Bode, W., Mayr, I., Baumann, U., Huber, R., Stone, S. R., and Hofsteenge, J. (1989) *EMBO J. 8*, 3467−3475.
36. Madison, E. L., Goldsmith, E. J., Gerard, R. D., Gething, M.-J. H., and Sambrook, J. F. (1989) *Nature 339*, 721−724.
37. Madison, E. L., Goldsmith, E. J., Gerard, R. D., Gething, M.-J. H., Sambrook, J. F., and Bassel-Duby, R. S. (1990) *Proc. Natl. Acad. Sci. U.S.A. 87*, 3530−3533.
38. Paoni, N. F., Chow, A. M., Peña, L. C., Keyt, B. A., Zoller, M. J., and Bennett, W. F. (1993) *Protein Eng. 6*, 529−534.
39. Bennett, W. F., Paoni, N. F., Keyt, B. A., Botstein, D., Jones, A. J. S., Presta, L., Wurm, F. M., and Zoller, M. J. (1991) *J. Biol. Chem. 266*, 5191−5201.
40. Gohlke, M., Baude, G., Nuck, R., Grunow, D., Kannicht, C., Bringmann, P., Donner, P., and Reutter, W. (1996) *J. Biol. Chem. 271*, 7381−7386.
41. Huber, R., and Bode, W. (1978) *Acc. Chem. Res. 11*, 114−122.
42. Tachias, K., and Madison, E. L. (1996) *J. Biol. Chem. 271*, 28749−28752.
43. Tachias, K., and Madison, E. L. (1997) *J. Biol. Chem. 272*, 28−31.
44. Lijnen, H. R., Van Hoef, B., and Collen, D. (1987) *Eur. J. Biochem. 162*, 351−356.
45. Powers, J. C. (1977) *Chemistry and Biochemistry of Amino Acids, Peptides and Proteins*, Vol. 4, pp 65−178, Marcel Decker, New York.
46. Evans, S. V. (1993) *J. Mol. Graphics 11*, 134−138.
47. Petersen, L. C., Boel, E., Johannessen, M., and Foster, D. (1990) *Biochemistry 29*, 3451−3457.

BI971129X